CHINESE OPTICS LETTERS

Vol. 19, No. 3 | March 2021

Interface and bulk controlled perovskite nanocrystal growth for high brightness light-emitting diodes [Invited]

Le Jiang (江 乐)[1], Xi Luo (罗 溪)[1], Zhongming Luo (罗钟明)[2], Dingjian Zhou (周定坚)[1], Baoxing Liu (刘宝星)[2], Jincheng Huang (黄金成)[2], Jianfeng Zhang (张建锋)[2], Xulin Zhang (张旭琳)[2], Ping Xu (徐 平)[2*], and Guijun Li (李贵君)[2**]

[1] College of Electronics and Information Engineering, Shenzhen University, Shenzhen 518060, China

[2] College of Physics and Optoelectronic Engineering, Shenzhen University, Shenzhen 518060, China

*Corresponding author: xuping@szu.edu.cn

**Corresponding author: gliad@connect.ust.hk

Received December 24, 2020 | Accepted January 27, 2021 | Posted Online March 9, 2021

Halide perovskites have attracted great attention due to their high color purity, high luminance yield, low non-radiative recombination rate, and solution processability. Although the external quantum efficiency of perovskite light-emitting diodes (PeLEDs) is comparable with that of the organic light-emitting diodes (OLEDs) and quantum-dots light-emitting diodes (QLEDs), the brightness is still low compared with the traditional OLEDs and QLEDs. Herein, we demonstrate high brightness and high-efficiency $CsPbBr_3$-based PeLEDs using interface and bulk controlled nanocrystal growth of the perovskite emission layer. The interface engineering by ethanolamine and bulk engineering by polyethylene glycol led to highly crystallized and cubic-shaped perovskite nanocrystals with smooth and compact morphology. As a result, PeLEDs with a high brightness of 64756 cd/m^2 and an external quantum efficiency of 13.4% have been achieved.

Keywords: perovskite; light-emitting diodes; morphology engineering; ethanolamine; polyethylene glycol.
DOI: 10.3788/COL202119.030001

1. Introduction

Halide perovskite luminescent materials have attracted great attention due to their high color purity (narrow emission spectrum), tunable emission color, and solution processibility[1–5]. In recent years, rapid progress has been made in realizing high-efficiency perovskite light-emitting diodes (PeLEDs). However, the widely reported high-efficiency PeLEDs are always in a low brightness state, and there are few studies based on this aspect, which is an essential issue in developing commercialized PeLEDs for display and lighting applications. To achieve high brightness and high external quantum efficiency (EQE) simultaneously for the PeLED, a strategy of enhancing the charge injection and charge radiative recombination is required, which can be realized by well-controlled perovskite emission layer (EML) nanocrystal morphology. Particularly, morphology plays a crucial role in the spatial confinement of perovskite with small and stable nanocrystals[6,7], reduction of possible current leakage, suppression of trap defect induced non-radiative recombination, etc.

For PeLED fabrication, the solution process is widely used. During the solution process, different solubility of organic solvents that dissolve the perovskite components and ion binding diversity in the solution make it difficult to control the directional crystallization of perovskite crystals[8–11]. In principle, the crystallization process is mainly affected by the coordination bond between crystal vacancies and functional groups of some additives[9,12,13]. Furthermore, when perovskite crystallizes during the spin coating process of a certain speed, defects such as pinholes, incomplete crystal grains, and irregular ions will inevitably be introduced. In order to increase the radiative recombination rate, defects should be suppressed, which are often passivated through morphology engineering or composition engineering by using various organic and inorganic additives[14–19]. Because the spin coating is conducted on a hole transporting layer (HTL) or an electron transporting layer (ETL), the surface chemical and physical properties of the underlying interlayers have an impact on the crystal growth process and thus the morphology of the perovskite EML. In addition, the additive of the perovskite precursor also plays an important role in the crystallization process.

In this article, we propose an interface and bulk method to control the $CsPbBr_3$ crystallization process. In terms of interface engineering, ethanolamine (ETA) is doped into the poly(3,4-ethylenedioxy-thiophene):poly-(styrenesulfonate) (PEDOT:PSS) HTL. The intermolecular interaction between the perovskite precursor and the amino-functionalized group of ETA promotes the cubic-shaped crystal growth and passivates halide

vacancies through the coordination bonding between the Pb^{2+} and amino ($-NH_2$) groups. In terms of bulk morphology engineering, macromolecular polyethylene glycol (PEG) is added to the perovskite precursor to locally confine the nanocrystals and fill pores for high-quality perovskite composite films. As a result, a high brightness of 64756 cd/m^2 and a high EQE of 13.4% have been achieved for the pure green $CsPbBr_3$ PeLED simultaneously.

2. Results and Discussion

First, we investigate the impact of the surface chemistries and conditions of HTL on the crystal growth of $CsPbBr_3$ perovskite. Here, HTL is PEDOT:PSS with a different ETA doping concentration. The volume ratio of ETA to PEDOT:PSS is set to be 0%, 0.2%, 0.4%, and 0.6%. Without adding ETA, 0% represents the perovskite EML prepared on PEDOT:PSS. The photoluminescence (PL) spectra of the perovskite EMLs prepared on different volume ratios of ETA/PEDOT:PSS are shown in Fig. 1(a). We can see that the PL intensity increases with the volume ratio of ETA/PEDOT:PSS, reaching the highest value at 0.4%. Continuously increasing the ETA volume concentration will decrease the PL intensity. Furthermore, the addition of ETA in PEDOT:PSS affects the luminescent peak position. With the ETA addition, the emission exhibits a blue shift from 518 nm (without ETA) to 515 nm (0.6%) [inset of Fig. 1(a)]. The PL quantum yield (PLQY) measurement is shown in Fig. 1(b), and it can be seen that the PLQY is only 20.2% without ETA addition, which increases to 31.6% at 0.4% ETA doping. The result of the PLQY is consistent with the PL intensity measurement, revealing that the enhancement of the luminescent property is attributed to the increase of the radiative efficiency (η_{rad}). In principle, the radiative efficiency is given by the following:

$$\eta_{rad} = \frac{1/\tau_{rad}}{1/\tau_{rad} + 1/\tau_{no\text{-}rad}}. \quad (1)$$

Here, τ_{rad} is the radiative recombination time constant, and $\tau_{non\text{-}rad}$ is the non-radiative recombination time constant. It is clear that the enhancement of the radiative efficiency can be due to either the enhancement of the radiative recombination or the suppression of the non-radiative recombination.

To shed light on the mechanism that dominates the improvement of the radiative efficiency, the effect of ETA modified

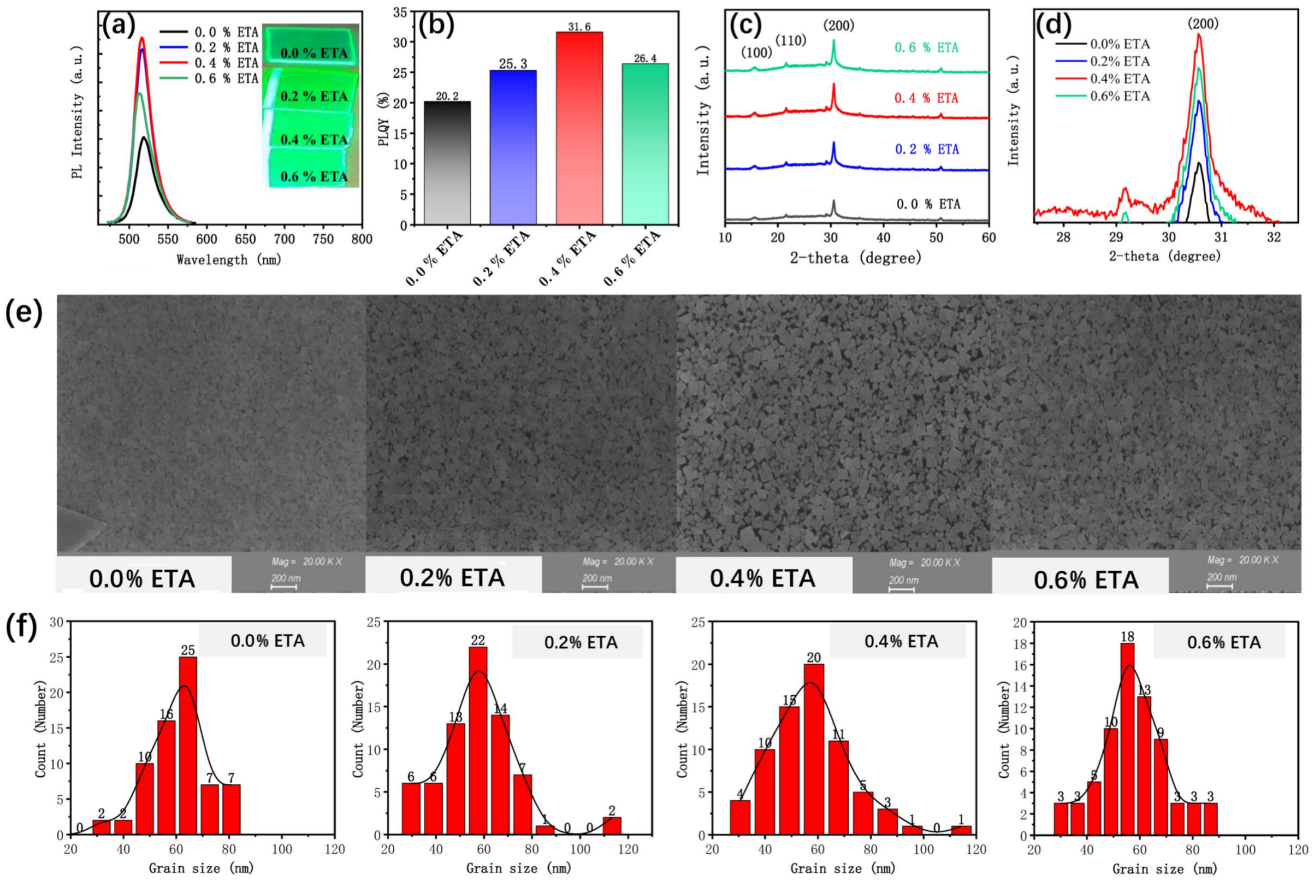

Fig. 1. Structural and optical characteristics of $CsPbBr_3$ perovskite films formed on the modified PEDOT:PSS with various ETA ratios. (a) Relative PL spectra and photos of different perovskite films under 400 nm illumination. (b) PLQY of PL. (c) XRD patterns. (d) XRD patterns of crystal orientation (200). (e) SEM images. (f) Grain size.

PEDOT:PSS on the perovskite film's crystal structure is measured by X-ray diffraction (XRD). A series of XRD spectra of the perovskite films is shown in Fig. 1(c). It can be seen that the XRD pattern of the perovskite films formed on the ETA-doped PEDOT:PSS is similar to that of the perovskite film formed on PEDOT:PSS without adding ETA, showing three typical characteristic peaks at 14.95°, 21.38°, and 30.30°, which correspond to the (100), (110), and (200) crystal planes of the cubic $CsPbBr_3$. The XRD pattern suggests a preferred crystallization along the (200) crystal plane, and its intensity increases with the increasing ETA concentration. However, when the ETA volume concentration is increased to 0.6%, the XRD intensity of the (200) plane decreases, as shown in Fig. 1(d). Figure 1(e) shows the scanning electron microscope (SEM) images of perovskites on different HTLs. The SEM images show remarkable changes in the morphology. When PEDOT:PSS is used, the perovskite shows large grains. The crystal grain growth is incomplete, and the grain distributes densely. With ETA addition, perovskite growth is complete, showing cubic-shaped nanocrystals with distinguished grain edges. However, when the volume ratio is increased to 0.6%, some of the grains collapse and convert from cubic to rectangular morphology. The change of the perovskite morphology is attributed to the improved surface wetting property and the molecular interaction between the ETA and perovskite precursor. Previous reports have suggested that the interaction can induce the deprotonation of the excess cations surrounding the corner sharing $[PbBr_6]^{4-}$ octahedron, giving rise to more uniform cubic-shaped nanocrystals[14]. The statistics of the grain size in Fig. 1(f) reveal that the main grain size of the nanocrystal grain decreases with the increasing ETA doping concentration. It seems that the tendency of the grain size contradicts the XRD results, as the XRD measurement shows increased crystallinity with the increasing ETA doping concentration for perovskite films. The increased crystallinity can then be attributed to the transformation of incomplete crystal growth towards more uniform cubic-shaped grains with a reduced grain boundary.

These results show that interface engineering with ETA can enhance perovskite crystallization and promote the passivation of defects. The enhanced radiative recombination can be attributed not only to the increased crystallinity, but also to the amino-functionalized group of ETA. ETA molecules have the amino ($-NH_2$) groups, which have the potential to passivate the surface halide vacancies through the coordination bonding between exposed Pb^{2+} and amino ($-NH_2$) groups[20]. As a result, the halide vacancies at the perovskite/HTL interface can be well passivated. The passivation leads to the suppression of the non-radiative recombination. Furthermore, it has been reported that the radiative recombination process of halide perovskite preferred to occur at the edge of the nanocrystal[21]. Because the perovskite EML prepared on the ETA-modulated HTL surface exhibits distinguished grain edges with reduced trap states, the edge emission characteristics also explain the enhancement of the radiative recombination.

The PeLED is prepared with PEDOT:PSS as the HTL and 2,2′,2′′-(1,3,5-benzinetriyl)-tris(1-phenyl-1-H-benzimidazole) (TPBi)/LiF as the ETL. Figure 2(a) is the schematic device structure of glass/$SnIn_2O_3$ (ITO, 100 nm)/HTL (30 nm)/perovskite (50 nm)/TPBi (50 nm)/LiF (1 nm)/Al (100 nm). Figure 2(b) shows the normalized electroluminescence (EL) spectra for PeLEDs. The emission peak of the ETA-modulated device shows a blue shift from 518 nm (without ETA doping) to 515 nm (0.4% and 0.6%), which is consistent with the variation of the PL spectra. The blue shift of the emission peak suggests the removal of the shallow traps of the perovskite EML. However, the blue shift may also be caused by changes in the perovskite grain size. The narrow emission width of 19 nm proves the high crystallinity of the perovskite nanocrystals. Figures 2(c)–2(f) show the characteristic EL performance of PeLEDs prepared on different HTLs.

The detailed luminescence data are shown in Table 1. The current density–voltage (*J-V*) in Fig. 2(c) and brightness–voltage (*L-V*) curves in Fig. 2(d) show that, under the same bias voltage, the current density and brightness of the PeLEDs with the ETA modified PEDOT:PSS (0.4% and 0.6%) are both higher than that of the device without using ETA. The increase of the current density injection for the ETA-modulated devices mainly originates from the porous morphology, giving rise to the high leakage current. Even then, high brightness of 27,968 cd/m^2 is still achieved for this porous morphological device, manifesting the enhanced radiative recombination and suppressed

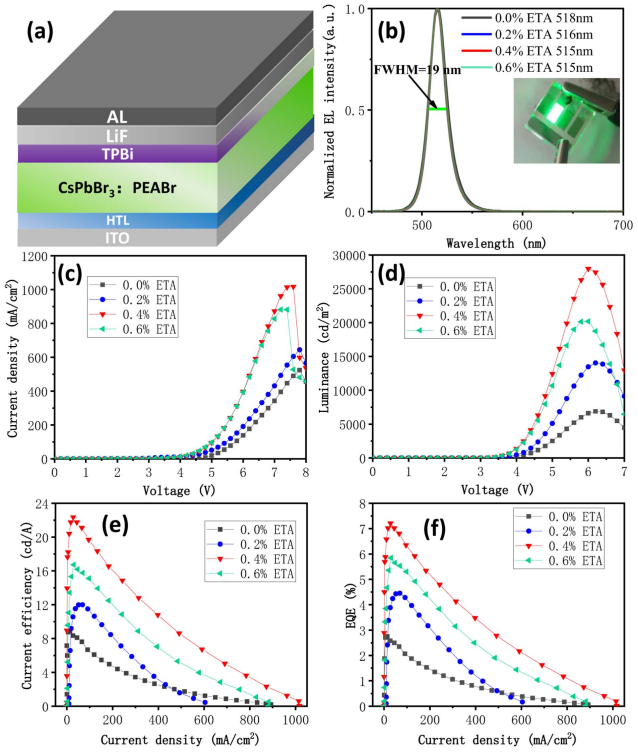

Fig. 2. Device performance of PeLEDs fabricated on ITO-glass with various ETA ratios in PEDOT:PSS. (a) Device structure of the PeLED. (b) EL spectrum for the PeLED with $CsPbBr_3$ as the EML. (c) *J-V* and (d) *L-V* characteristics. (e) CE as a function of luminance. (f) EQE as a function of luminance.

Table 1. Summary of the EL Performance of the PeLEDs with Different ETA Doping Concentrations.

ETA Ratio (%)	Luminance (cd/m^2)/ Voltage (V)	CE (cd/A)	EQE (%)/ Voltage (V)
0.0	6897/6.2	8.88	2.75/4.0
0.2	14,037/6.2	11.99	4.45/5.0
0.4	27,968/6.2	22.35	7.21/4.2
0.6	20,198/6.0	16.72	5.84/4.2

non-radiative recombination. The high brightness gives rise to high current efficiency (CE) of 22.35 cd/A and high EQE of 7.21% [Figs. 2(e) and 2(f)], both of which are obtained when the ETA doping ratio is 0.4%, agreeing with the PL and PLQY results.

Although interfacial engineering with ETA-modulated PEDOT:PSS results in the growth of cubic-shaped nanocrystals with high crystallinity, the porous morphology may also lead to current leakage due to the direct contact between HTL and ETL. Therefore, it is necessary to control the bulk perovskite growth towards a more compact morphology. Therefore, we further introduce the macromolecular polymer PEG into the perovskite precursor. The as-obtained PEG-doped perovskite film exhibits high brightness, as can be seen from the inset of Fig. 3(a). The enhanced brightness is characterized by the PL measurement. With PEG doping, the PL intensity increases, reaching a maximum value at a doping concentration of 20 mg/mL. A high doping concentration of 30 mg/mL decreases the PL intensity. The optimal doping concentration of 20 mg/mL corresponds to a maximum PLQY of 54.8%, compared with a value of 39% for perovskite without PEG doping [Fig. 3(b)].

To further understand the improvement of PL properties with PEG doping, XRD and SEM are used to illustrate the changes of crystallinity and morphology of perovskite films [Figs. 3(c), 3(d), and 3(e)]. There are three prominent diffraction peaks at 14.95°, 21.38°, and 30.30°, which correspond to the (100), (110), and (200) crystal planes, respectively. With PEG doping, the XRD peak position does not change. However, the crystallinity decreases with the increase of the PEG concentration. The peak intensity increases again when the PEG concentration increases to 30 mg/mL. The decrease of the crystallinity is a result of the reduction of the grain size, as revealed by the SEM images [Fig. 3(e)]. The grain size statistics in Fig. 3(f) demonstrate that the main grain size reduces from 70 nm (0 mg/mL PEG) to 60 nm (10 mg/mL) to 40 nm (20 mg/mL). Large-sized crystal particles appear when the PEG concentration is 30 mg/mL, which is supported by the increased crystallinity from the XRD spectrum. In addition to the decreased XRD intensity, another apparent feature from the SEM result is that the perovskite film becomes dense and compact when decreasing the grain size with PEG. It is well known that PEG is a Lewis base,

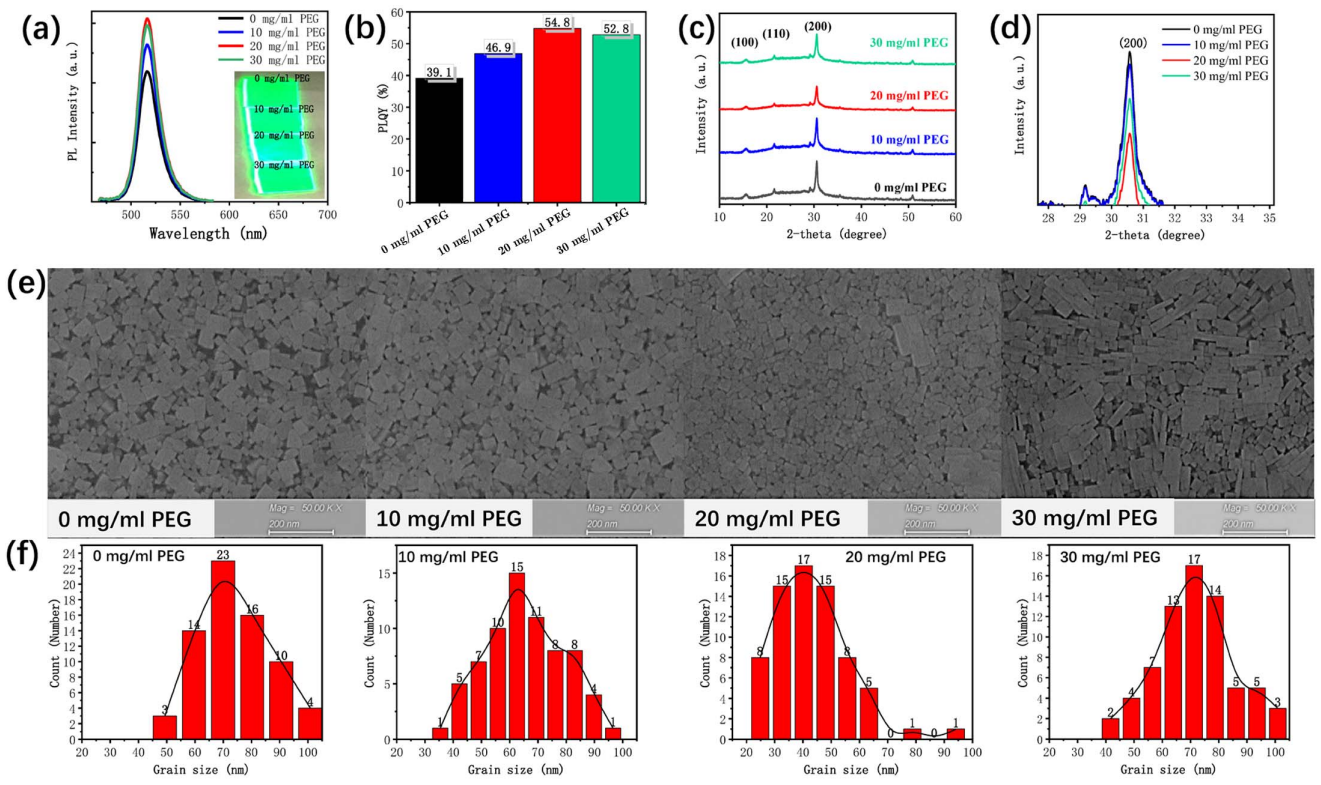

Fig. 3. Structural and optical characteristics of $CsPbBr_3$ perovskite films with various PEG ratios. (a) Relative PL spectra and photos of different perovskite films under 400 nm illumination. (b) PLQY of PL. (c) XRD patterns. (d) XRD patterns of crystal orientation (200). (e) SEM images. (f) Grain size.

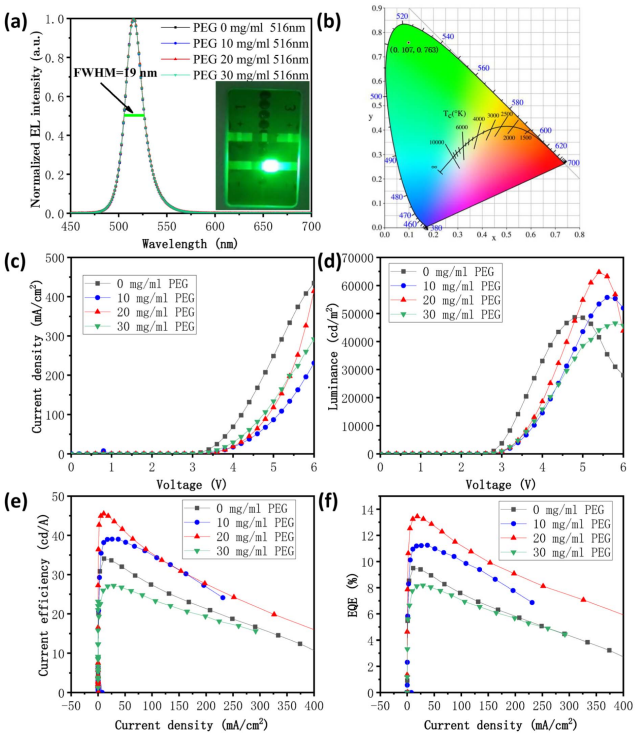

Fig. 4. (a) EL spectrum for the PeLED with PEG:$CsPbBr_3$ as the EML. (b) The 1931 International Commission on Illumination (CIE) color coordinate. (c) *J-V* and (d) *L-V* characteristics. (e) CE as a function of luminance. (f) EQE as a function of luminance.

which can coordinate with the lead ions of perovskite, which is considered to facilitate passivating the point defects and enhancing the luminescence of perovskite. Additionally, the growth of perovskite crystal is confined within a localized space and cross-links the grain size to obtain a smooth and compact morphology, which helps to reduce the leakage current.

PeLEDs are fabricated to evaluate the effect of the perovskite nanocrystal morphology on the device performance. As shown in Fig. 4(a), all devices exhibit the same emission spectrum centered at 516 nm, along with a narrow emission width of 19 nm. It is a pure green emission with the International Commission on Illumination (CIE) coordinates of (0.107,0.763) [Fig. 4(b)]. Figures 4(c)–4(f) are the characteristic performances including *J-V*, *L-V*, CE-*J*, and EQE-*J*. From the *J-V* curves [Fig. 4(c)], we can see that the PEG doping largely decreases the leakage current because of the dense and compact morphology that prevents direct contact between HTL and ETL. For 10 mg/mL and 20 mg/mL PEG doping concentrations, the brightness is enhanced [Fig. 4(d)]. However, the high CE is only obtained at the PEG doping concentration of 20 mg/mL, manifesting that the leakage current is successfully inhibited only with the dopant condition of 20 mg/mL. Table 2 summarizes the device parameter obtained from Figs. 4(c)–4(f). Without PEG, the device exhibits a maximum brightness of 48,529 cd/m^2, a maximum CE of 34.08 cd/A, and a peak EQE of 9.49%. With PEG doping, the turn-on voltage (V_{on}) is reduced from 2.8 V to 2.6 V. With 20 mg/mL PEG, the device shows a maximum brightness of 64,756 cd/m^2 at 5.4 V, CE of 45.52 cd/A, and 13.44% maximum EQE.

Table 2. EL Performance of the PeLEDs with Different PEG Concentrations in Perovskite-Emitting Layers.

PEG Concentration (mg/mL)	Luminance (cd/m^2)/ Voltage (V)	CE (cd/A)	EQE (%)/ Voltage (V)
0.0	48,529/4.8	34.08	9.49/3.8
10.0	55,736/5.6	39.04	11.24/3.6
20.0	64,756/5.4	45.52	13.44/3.4
30.0	46,554/5.8	27.16	8.17/4.0

In summary, we have demonstrated the interface and bulk control of the morphology of the perovskite nanocrystals toward high brightness and high-efficiency PeLEDs. The ETA-modulated PEDOT:PSS interface approach confirmed the critical role of the interfacial effect on perovskite crystallization and defect passivation. ETA-doped PEDOT:PSS triggered the formation of high-quality perovskite films with high crystallinity and cubic-shaped nanocrystals, resulting in the enhancement of the radiative recombination and the suppression of the non-radiative losses. The bulk approach using macromolecular polymer PEG as the dopant of the perovskite precursor successfully improved perovskite EML with a smooth and compact morphology and reduced the leakage current by preventing the direct contact between ELT and HTL. These results provide a new defect passivation method for improving perovskite LEDs' performance and have a particular significance for the development of other perovskite-based electronic devices.

3. Experimental Section

Materials. Cesium bromide (CsBr, 99.0%), lead bromide ($PbBr_2$, 99.0%), and phenethylammonium bromide (PEABr) were purchased from Xi'an Polymer Light Technology Corp. 1,4,8,11-tetraazacyclotetradecane (cyclam) and trioctylphosphine oxide (TOPO) were purchased from Macklin. TPBi (99%), dimethyl sulfoxide (DMSO, anhydrous, 99.9%), chlorobenzene (CB, 99.9%), PEG (Mv~600,000), ETA (99.5%), and LiF (99.99%) were purchased from Aladdin Industrial Corporation. All materials are used directly without any purification treatment.

Perovskite Film Fabrication. 63.8 mg CsBr, 113.7 mg $PbBr_2$, 30 mg PEABr, and 2 mg cyclam were mixed and dissolved in 1 mL DMSO to obtain a 0.31 mol/L perovskite precursor solution with PEG of 0, 10, 20, and 30 mg/mL. The precursor was placed on a hot plate, stirring for 12 h at 50°C. Before use, it was filtered with a 0.22 μm polytetrafluoroethylene (PTFE) filter. The perovskite EML was obtained by spin coating at 5000 r/min for 45 s, and 0.5 mg/mL TOPO CB solution was used

to passivate the perovskite, which was introduced during the anti-solvent process. The perovskite was put on a hot plate at 60°C for 15 min. The preparation process of the perovskite film was completed in a N_2 atmosphere glove box.

LED Fabrication. Firstly, the ITO glass substrate was cleaned with deionized water, detergent, deionized water, isopropanol, and acetone in order with a water temperature of 40°C and 100% intensity ultrasonic cleaning, and then placed in an oven at 100°C for 1 h. Before the deposition of PEDOT:PSS, the ITO substrate was placed under a UVO_3 cleaner for 10 min. The HTL was prepared by the spin coating of the PEDOT:PSS solution or modified solution (with ETA) at 4000 r/min for 45 s; finally, the sample was put on the hot plate and annealed at 150°C for 30 min. The sample is transferred into the glove box to deposit the perovskite EML. TPBi, LiF, and Al electrodes were deposited using a high thermal evaporation system. The thicknesses of TPBi, LiF, and Al are 45 nm, 0.9 nm, and 100 nm, respectively.

Characterization Measurements. The surface morphology of the $CsPbBr_3$ film was observed by SEM (RAITH, EBPG5200), and the crystallization condition of the perovskite film was obtained by an X-ray powder diffractometer (Rigaku, MiniFlex600). The current-luminance-voltage (*I-L-V*) characteristic curve of PeLEDs was measured by the EL measurement system Enlitech. All films and devices measurement and characterization were performed in an atmospheric environment at room temperature.

PLQY. The PLQY is defined as the ratio of photons absorbed to photons emitted through PL. In other words, the quantum yield gives the probability of the excited state being deactivated by PL rather than by other, non-radiative mechanisms.

PLQY = Photon emitted/Photon absorbed. (The minimum measurement value can be 0.1%.)

The PLQY of the perovskite films was measured using Enlitech LQ-100X equipment with a 450 W xenon lamp as the excitation source. The following settings were applied for PLQY measurements: excitation wavelength of 400 nm, laser delay of 20 ms, and source delay of 2000 ms, respectively, with step increments of 1 nm. We measured the light intensity with a laser power meter, and the estimated light power density incident on the samples was about 4.5 mW/cm^2.

Acknowledgement

This work was financially supported by the National Natural Science Foundation of China (No. 61804097), the Natural Science Foundation of Guangdong Province (No. 2020A1515010792), and the Science and Technology Program of Shenzhen (No. SGDX20190918105001787).

References

1. Z. B. Wang, T. Cheng, F. Z. Wang, S. Y. Dai, and Z. A. Tan, "Morphology engineering for high-performance and multicolored perovskite light-emitting diodes with simple device structures," Small **12**, 4412 (2016).
2. Y. Tian, Y. C. Ling, Y. Shu, C. K. Zhou, T. Besara, T. Siegrist, H. W. Gao, and B. W. Ma, "A solution-processed organometal halide perovskite hole transport layer for highly efficient organic light-emitting diodes," Adv. Electron. Mater. **2**, 1600165 (2016).
3. H. C. Cho, S. H. Jeong, M. H. Park, Y. H. Kim, C. Wolf, C. L. Lee, J. H. Heo, A. Sadhanala, N. Myoung, S. Yoo, S. H. Im, R. H. Friend, and T. W. Lee, "Overcoming the electroluminescence efficiency limitations of perovskite light-emitting diodes," Science **350**, 1222 (2015).
4. C. T. Wang, K. Chen, P. Xu, F. Yeung, H. S. Kwok, and G. Li, "Fully chiral light emission from $CsPbX_3$ perovskite nanocrystals enabled by cholesteric superstructure stacks," Adv. Funct. Mater. **29**, 1903155 (2019).
5. J. Zhang, C. Meng, J. Huang, L. Jiang, D. Zhou, R. Chen, F. Yeung, H.-S. Kwok, P. Xu, and G. Li, "Strong linearly polarized photoluminescence and electroluminescence from halide perovskite/azobenzene dye composite film for display applications," Adv. Opt. Mater. **8**, 1901824 (2020).
6. J. C. Yu, D. W. Kim, D. B. Kim, E. D. Jung, J. H. Park, A.-Y. Lee, B. R. Lee, D. D. Nuzzo, R. H. Friend, and M. H. Song, "Improving the stability and performance of perovskite light-emitting diodes by thermal annealing treatment," Adv. Mater. **28**, 6906 (2016).
7. H. Cho, S.-H. Jeong, M.-H. Park, Y.-H. Kim, C. Wolf, C.-L. Lee, J. H. Heo, A. Sadhanala, N. S. Myoung, S. Yoo, S. H. Im, R. H. Friend, and T.-W. Lee, "Overcoming the electroluminescence efficiency limitations of perovskite light-emitting diodes," Science **350**, 1222 (2015).
8. J. Wu, J. Shi, Y. Li, H. Li, H. Wu, Y. Luo, D. Li, and Q. Meng, "Quantifying the interface defect for the stability origin of perovskite solar cells," Adv. Energy Mater. **9**, 1901352 (2019).
9. M. L. Agiorgousis, Y. Y. Sun, H. Zeng, and S. Zhang, "Strong covalency-induced recombination centers in perovskite solar cell material $CH_3NH_3PbI_3$," J. Am. Chem. Soc. **136**, 14570 (2014).
10. G. Li, K. L. Ching, J. Y. L. Ho, M. Wong, and H.-S. Kwok, "Identifying the optimum morphology in high-performance perovskite solar cells," Adv. Energy Mater. **5**, 1401775 (2015).
11. J. Zhang, B. Ren, S. Deng, J. Huang, L. Jiang, D. Zhou, X. Zhang, M. Zhang, R. Chen, F. Yeung, H.-S. Kwok, P. Xu, and G. Li, "Voltage-dependent multicolor electroluminescent device based on halide perovskite and chalcogenide quantum-dots emitters," Adv. Funct. Mater. **30**, 1907074 (2019).
12. Y. Lin, L. Shen, J. Dai, Y. Deng, Y. Wu, Y. Bai, X. Zheng, J. Wang, Y. Fang, H. Wei, W. Ma, X. C. Zeng, X. Zhan, and J. Huang, "π-conjugated Lewis base: efficient trap-passivation and charge-extraction for hybrid perovskite solar cells," Adv. Mater. **29**, 1604545 (2017).
13. D. W. Dequilettes, S. Koch, S. Burke, R. Paranji, A. J. Shropshire, M. E. Ziffer, and D. S. Ginger, "Photoluminescence lifetimes exceeding 8 μs and quantum yields exceeding 30% in hybrid perovskite thin films by ligand passivation," ACS Energy Lett. **1**, 438 (2016).
14. Z. Yuan, Y. Miao, Z. Hu, W. Xu, C. Kuang, K. Pan, P. Liu, J. Lai, B. Sun, J. Wang, S. Bai, and F. Gao, "Unveiling the synergistic effect of precursor stoichiometry and interfacial reactions for perovskite light-emitting diodes," Nat. Commun. **10**, 2818 (2019).
15. M. Yuan, L. N. Quan, R. Comin, G. Walters, R. Sabatini, O. Voznyy, S. Hoogland, Y. Zhao, E. M. Beauregard, P. Kanjanaboos, Z. Lu, D. H. Kim, and E. H. Sargent, "Perovskite energy funnels for efficient light-emitting diodes," Nat. Nanotechnol. **11**, 872 (2016).
16. S. A. Veldhuis, Y. F. Ng, R. Ahmad, A. Bruno, N. F. Jamaludin, B. Damodaran, N. Mathews, and S. G. Mhaisalkar, "Crown ethers enable room temperature synthesis of $CsPbBr_3$ quantum dots for light-emitting diodes," ACS Energy Lett. **3**, 526 (2018).
17. S. Kumar, J. Jagielski, N. Kallikounis, Y. H. Kim, C. Wolf, F. Jenny, T. Tian, C. J. Hofer, Y.-C. Chiu, W. J. Stark, T.-W. Lee, and C.-J. Shih, "Ultrapure green light-emitting diodes using two-dimensional formamidinium perovskites: achieving recommendation 2020 color coordinates," Nano Lett. **17**, 5277 (2017).
18. Y. Cao, N. Wang, H. Tian, J. Guo, Y. Wei, H. Chen, Y. Miao, W. Zou, K. Pan, Y. He, H. Cao, Y. Ke, M. Xu, Y. Wang, M. Yang, K. Du, Z. Fu, D. Kong, D. Dai, Y. Jin, G. Li, H. Li, Q. Peng, J. Wang, and W. Huang, "Perovskite light-emitting diodes based on spontaneously formed submicrometre-scale structures," Nature **562**, 249 (2018).
19. B. Ren, G. Yuen, S. Deng, L. Jiang, D. Zhou, L. Gu, P. Xu, M. Zhang, Z. Fan, F. Sze, Y. Yueng, R. Chen, H.-S. Kwok, and G. Li, "Multifunctional

optoelectronic device based on an asymmetric active layer structure," Adv. Funct. Mater. **29**, 1807894 (2019).
20. W. Xu, Q. Hu, S. Bai, C. Bao, Y. Miao, Z. Yuan, T. Borzda, A. J. Barker, E. Tyukalova, Z. Hu, M. Kawecki, H. Wang, Z. Yan, X. Liu, X. Shi, K. Uvdal, M. Fahlman, W. Zhang, M. Duchamp, J.-M. Liu, A. Petrozza, J. Wang, L.-M. Liu, W. Huang, and F. Gao, "Rational molecular passivation for high-performance perovskite light-emitting diodes," Nat. Photon. **13**, 418 (2019).
21. K. Wang, C. Wu, Y. Jiang, D. Yang, K. Wang, and S. Priya, "Distinct conducting layer edge states in two-dimensional (2D) halide perovskite," Sci. Adv. **5**, eaau3241 (2019).